11-10-2016

# 125Te NMR and Seebeck Effect in Bi2Te3 Synthesized from Stoichiometric and Te-Rich Melts

E. M. Levin
*Iowa State University and Ames Laboratory*

Trevor M. Riedemann
*Ames Laboratory*, tmr@ameslab.gov

A. Howard
*Ames Laboratory*

Na Hyun Jo
*Iowa State University*, njo@iastate.edu

Sergey L. Bud'ko
*Iowa State University and Ames Laboratory*, budko@ameslab.gov

*See next page for additional authors*

# 125Te NMR and Seebeck Effect in Bi2Te3 Synthesized from Stoichiometric and Te-Rich Melts

**Abstract**

Bi2Te3 is a well-known thermoelectric material and, as a new form of quantum matter, a topological insulator. Variation of local chemical composition in Bi2Te3 results in formation of several types of atomic defects, including Bi and Te vacancies and Bi and Te antisite defects; these defects can strongly affect material functionality via generation of free electrons and/or holes. Nonuniform distribution of atomic defects produces electronic inhomogeneity, which can be detected by 125Te nuclear magnetic resonance (NMR). Here we report on 125Te NMR and Seebeck effect (heat to electrical energy conversion) for two single crystalline samples: (#1) grown from stoichiometric composition by Bridgman technique and (#2) grown out of Te-rich, high temperature flux. The Seebeck coefficients of these samples show p- and n-type conductivity, respectively, arising from different atomic defects. 125Te NMR spectra and spin–lattice relaxation measurements demonstrate that both Bi2Te3 samples are electronically inhomogeneous at the atomic scale, which can be attributed to a different Te environment due to spatial variation of the Bi/Te ratio and formation of atomic defects. Correlations between 125Te NMR spectra, spin–lattice relaxation times, the Seebeck coefficients, carrier concentrations, and atomic defects are discussed. Our data demonstrate that 125Te NMR is an effective probe to study antisite defects in Bi2Te3.

**Disciplines**

Biological and Chemical Physics | Materials Chemistry | Materials Science and Engineering | Physical Chemistry

**Comments**

This document is the Accepted Manuscript version of a Published Work that appeared in final form in *The Journal of Physical Chemistry C*, copyright © American Chemical Society after peer review and technical editing by the publisher. To access the final edited and published work see DOI: 10.1021/acs.jpcc.6b06973. Posted with permission.

**Authors**

E. M. Levin, Trevor M. Riedemann, A. Howard, Na Hyun Jo, Sergey L. Bud'ko, Paul C. Canfield, and Thomas A. Lograsso

10-11-2016

# $^{125}$Te NMR and Seebeck Effect in $Bi_2Te_3$ Synthesized from Stoichiometric and Te-rich Melts

E. M. Levin,[1,2*] T. M. Riedemann,[1] A. Howard,[1] N. H. Jo,[2] S. L. Bud'ko,[1,2]
P. C. Canfield,[1,2] and T. A. Lograsso[1,3]

[1] *Division of Materials Sciences and Engineering, U.S. Department of Energy Ames Laboratory, Ames, Iowa 50011, USA*
[2] *Department of Physics and Astronomy, Iowa State University, Ames, Iowa 50011, USA*
[3] *Department of Materials Science and Engineering, Iowa State University, Ames, Iowa 50011, USA*

Submitted to *J. of Physical Chemistry C*

## Abstract

$Bi_2Te_3$ is a well-known thermoelectric material and as a new form of quantum matter, a topological insulator. Variation of local chemical composition in $Bi_2Te_3$ results in formation of several types of atomic defects, including Bi and Te vacancies, and Bi and Te antisite defects; these defects can strongly affect material functionality via generation of free electrons and/or holes. Non-uniform distribution of atomic defects produces electronic inhomogeneity, which can be detected by $^{125}$Te nuclear magnetic resonance (NMR). Here we report on $^{125}$Te NMR and Seebeck effect (heat to electrical energy conversion) for two single crystalline samples: (#1) grown from stoichiometric composition by Bridgman technique, and (#2) grown out of Te-rich, high temperature flux. The Seebeck coefficients of these samples show *p*- and *n*-type conductivity, respectively, arising from different atomic defects. $^{125}$Te NMR spectra and spin-lattice relaxation measurements demonstrate that both $Bi_2Te_3$ samples are electronically inhomogeneous at the atomic scale, which can be attributed to a different Te environment due to spatial variation of the Bi/Te ratio and formation of atomic defects. Correlations between $^{125}$Te NMR spectra, spin-lattice relaxation times, the Seebeck coefficients, carrier concentrations, and atomic defects are discussed. Our data demonstrates that $^{125}$Te NMR is an effective probe to study antisite defects in $Bi_2Te_3$.

## 1. INTRODUCTION

$Bi_2Te_3$ is a narrow band gap semiconductor well-known for its utilization in refrigerating devices due to its large Peltier effect.[1] $Bi_2Te_3$ has been studied for a long time and various experimental methods have been used to better understand this interesting material. [1-3] Recently, $Bi_2Te_3$ was considered as a new form of quantum matter, a three-dimensional topological insulator, which stimulates its study as a material for possible spintronic and quantum computing applications.[2,3] The bulk electrical conductivity of $Bi_2Te_3$ is very sensitive to defects whose occurrence is dependent on the composition and synthesis method. Detailed studies, using several experimental methods, are required to better understand this and related materials.

One of the microscopic techniques used to study complex tellurides, e.g., PbTe- and GeTe-based materials, is nuclear magnetic resonance (NMR). It has been shown that $^{207}Pb$[4,5] and $^{125}Te$ NMR[5-8] spectra and spin-lattice relaxation measurements enable detection of different chemical environments and determination of the carrier concentration. Micro- [9] and nano-size [10] powder $Bi_2Te_3$ samples were also studied by $^{125}Te$ NMR. Taylor *et al*.[9] have shown that $^{125}Te$ NMR spectrum of micro-size powder $Bi_2Te_3$ ground by mortar and pestle contains one peak at about +400 ppm (parts per $10^6$). It was stated that $^{125}Te$ NMR of micro-size grains reflects properties of bulk $Bi_2Te_3$.[9] Koumoulis *et al*. [10] have shown that $^{125}Te$ NMR spectra of nano-scale particles of $Bi_2Te_3$ prepared by ball-milling contain a main peak at +500 ppm, and in addition, a shoulder at -500 ppm. Unfortunately, the details on the initial bulk samples synthesis and their properties were not reported, but the authors suggest that the size of grains can strongly affect $^{125}Te$ NMR spectra.

Earlier, we have shown that $^{125}Te$ NMR enables a better understanding of the chemistry and physics of GeTe- and PbTe-based tellurides related to atomic defects.[5,6,8] It is also well

known that the Bi/Te ratio in $Bi_2Te_3$ produces a strong effect on electronic properties via formation of various atomic defects,[11] acting even stronger than in GeTe- and PbTe-based materials. Here we report on $^{125}$Te NMR spectra and spin-lattice relaxation measurements along with the Seebeck coefficient and Hall effect measurements for two single crystalline $Bi_2Te_3$ samples, and discuss the effects arising from atomic defects. The samples were prepared by different methods, (i) by Bridgman method from a starting composition of stoichiometric $Bi_2Te_3$, and (ii) grown out of Te-rich high temperature flux.

## 2. EXPERIMENTAL DETAILS

Two $Bi_2Te_3$ samples (#1 and #2) were synthesized using high purity components, 99.999% Bi and 99.999% Te. $Bi_2Te_3$ (#1) was synthesized by direct melting of constituent components with initial stoichiometry $Bi_{40}Te_{60}$ in a 12 mm diameter fused silica ampoule at 650 $^oC$ for one hour, stirring periodically. The ingot was then placed in a 15 mm diameter fused silica crucible in argon back-filled up 250 mm Hg pressure atmosphere, sealed, and used for Bridgman single crystal growth at 800 $^oC$ with the withdrawal rate of 1 mm/hr. $Bi_2Te_3$ (#2) was grown out of Te-rich melt with initial stoichiometry of $Bi_{25}Te_{75}$ in an alumina crucible. The crucible was sealed in fused silica ampoule [12,13] and heated to 580 $^oC$ over 3 h, held at 580 $^oC$ for 3 h, slowly cooled down to 440 $^oC$ within 60 h, and then decanted using a centrifuge.[12,13] Details about solidification of $Bi_2Te_3$ from the melts of two initial nominal compositions, $Bi_{40}Te_{60}$ and $Bi_{25}Te_{75}$, can be seen on a Bi-Te phase diagram.[14]

XRD patterns were obtained using a Panalytical X'Pert Pro MPD system with Co-$K\alpha$ radiation ($\lambda$ = 0.1789 nm) at 300 K; both $Bi_2Te_3$ samples are found to be single-phase (Figure 1). $Bi_2Te_3$ crystallizes in the hexagonal structure with three planes, each containing five-atom $Te_{(1)}$-

Bi-$Te_{(2)}$-Bi-$Te_{(1)}$ layers, where Te atoms in the same plane are located in positions $Te_{(1)}$ and $Te_{(2)}$;[15] the structure can be described in terms of hexagonal [16] or rhombohedral structure.[15,17] Lattice parameters of our samples calculated using Rietveld refinements in the program X'Pert HighScore Plus [7] for both hexagonal and rhombohedral structures are shown in Table 1. Note that for $Bi_2Te_3$ (#2) the main Bragg peak is slightly shifted compared to that for $Bi_2Te_3$ (#1) (Fig. 1), and calculated lattice parameters are slightly smaller (see Table 1 and discussion below).

$^{125}$Te nuclear magnetic resonance (NMR) experiments were conducted at 126 MHz using a Bruker 400WB plus spectrometer with TopSpin software in a magnetic field of 9.4 T without sample spinning (static regime). Ten $\pi/2$ pulses with duration of 3 μs were used for saturating the magnetization. Signals were detected after a Hahn echo generated by a 2 μs and 3 μs pulse sequence.[5,7,18] $^{125}$Te NMR chemical shifts were referenced to $Te(OH)_6$ in solution and chemical shifts relative to $(CH_3)_2Te$ in benzene were larger by +712 ppm.[18] $^{125}$Te NMR spin-lattice relaxation measurements were used to obtain the spin-lattice relaxation time, $T_1$, and the free (mobile) charge carrier concentration. Saturated recovery time (delay time) was varied from 0.05 to 5000 ms, the number of scans for each delay time was 32k; total measurement time for each sample was about 200 hr. Fitting of the relaxation curves was conducted as described in Ref. 7.

The Seebeck coefficient was measured in the temperature range of 300-700 K using an LSR-3 measuring system (Linseis, Inc.). The time for each measurement was about 4 hours, and measurements were repeated several times in order to check the Seebeck coefficient stability. The measurements uncertainty is ~5%, and no hysteresis in the Seebeck coefficient during temperature cycling was observed. The Hall effect was measured at 300 K using a Quantum Design Physical Properties Measuring System, with the odd in magnetic field data taken as Hall

component. The carrier concentration was estimated from the linear fit magnetic field dependent Hall resistivity in the limit of low magnetic fields.

## 3. RESULTS AND DISCUSSION

Several different atomic defects are, in general, possible in $Bi_2Te_3$: (i) vacancies on the Bi sublattice, denoted as $V_{Bi}$, (ii) vacancies on the Te sublattice, denoted as $V_{Te}$, (iii) Bi antisite defects (Bi atom substitution of Te atom in the Te sublattice), denoted as $Bi_{Te}$, (iv) Te antisite defects (Te atom substitution of Bi atom in the Bi sublattice), denoted as $Te_{Bi}$, and (v) interstitial Bi or Te atoms.[3,19-22] It was shown experimentally by Fleurial *et al*.[11] that depending on the type of defects, which may generate free (mobile) electrons and/or holes, the Seebeck and Hall coefficients can be positive or negative, and different in the magnitude. Atomic defects in $Bi_2Te_3$ were also studied theoretically and discussed in detail by Scalon *et al*.[3] and by Hashibon and Elsasser. [23]

Figure 2 shows temperature dependencies of the Seebeck coefficient of $Bi_2Te_3$ (#1) and $Bi_2Te_3$ (#2). Since the other measurements in this work were performed at 300 K, through the rest of the paper we will refer, in the case of comparison, to the Seebeck coefficient at 300 K. The Seebeck coefficients of $Bi_2Te_3$ (#1) and $Bi_2Te_3$ (#2) are +250 $\mu V\ K^{-1}$ and -133 $\mu V\ K^{-1}$, respectively. Any difference found was within the error of measurements for the Seebeck coefficient of both samples between the first and second runs. The sign of the Seebeck coefficient shows that $Bi_2Te_3$ (#1) is *p*-type (conductivity due to holes), $Bi_2Te_3$ (#2) is *n*-type (conductivity due to electrons).

Scanlon *et al*.[3] suggested that antisite defects in $Bi_2Te_3$ in both cases, Bi-rich/Te-poor and Bi-poor/Te-rich, dominate over all other defects including anion and cation vacancies. Tellurium

antisite defects, $Te_{Bi}$, with the lowest formation energy of all possible defects in $Bi_2Te_3$ serve as donors and generate electrons with possible compensation by the $V_{Bi}$ defects, which serve as acceptors and generate holes.[3] In our sample $Bi_2Te_3$ (#2) synthesized from the melt with initial composition of $Bi_{25}Te_{75}$, the contribution from $Te_{Bi}$ defects overcomes those produced by other possible defects.

Bismuth antisite defects, $Bi_{Te}$, serve as acceptors and generate holes,[3] whereas $V_{Te}$ defects serve as donors. In sample $Bi_2Te_3$ (#1) synthesized from the melt with initial composition of $Bi_{40}Te_{60}$, the contribution from $Bi_{Te}$ defects overcomes those produced by other possible defects. In both cases, the type of conductivity in $Bi_2Te_3$ is determined by antisite defects, which agrees well with experimental data by Fleurial *et al*.[11] and theoretical modeling by Scalon *et al*. [3] Both types of antisite defects in our samples are thermally stable, which is demonstrated by similar temperature dependencies of the Seebeck coefficient during the first and following runs (Fig. 2).

Slightly smaller lattice parameters of Te-rich $Bi_2Te_3$ (#2) compared to that of $Bi_2Te_3$ (#1) (Table 1) should be attributed to the smaller atomic radii of Te, 0.14 nm, compare to that of Bi, 0.16 nm,[22] which can be present on regular site Te and Bi sites as well as on $Te_{Bi}$ and $Bi_{Te}$ antisites, respectively. This reflects variation in Bi/Te ratio that results from the different growth methods. It is to be expected that there is some width of formation for $Bi_2Te_3$, especially at high temperatures where growth occurs and solution growth from Te-rich melt will naturally produce a slightly Te enriched composition compared to a stoichiometric growth. This deviation is clearly reflected in all the measurements (see below).

Our Hall effect measurements show the *p*- and *n*-type conductivity of $Bi_2Te_3$ (#1) and $Bi_2Te_3$ (#2), and the carrier concentration of $1.2\times10^{19}$ holes/cm$^3$ and $3.0\times10^{19}$ electrons/cm$^3$, respectively (Table 2). Within the model for the Seebeck coefficient of metals and degenerate

semiconductors with energy independent scattering, $S \sim 1/n^{2/3}$, where $n$ is the carrier concentration.[24] To compare the Seebeck coefficients and carrier concentrations we can use the relation $S_{\#1} / S_{\#2} = (n_{\#2} / n_{\#1})^{2/3}$. The absolute value of the ratio $S_{\#1} / S_{\#2} = 250\ \mu V\ K^{-1}/133\ \mu V\ K^{-1} = 1.88$ results in $n_{\#2}/n_{\#1} = 2.56$, which agrees well with that obtained from the Hall effect measurements, 2.50, and reflects different concentrations of atomic defects affecting the total charge carrier concentration. Hence, the larger absolute value of the Seebeck coefficient of $Bi_2Te_3$ (#1) at 300 K compared to that of $Bi_2Te_3$ (#2) is mostly determined by the lower carrier concentration and can be attributed to lower concentration of antisite defects.

Figure 3 shows $^{125}$Te NMR spectra of $Bi_2Te_3$ (#1) (Fig. 3a) and $Bi_2Te_3$ (#2) (Fig. 3b). The spectra of both samples exhibit the main peak and the right shoulder. The main peak of $^{125}$Te NMR for $Bi_2Te_3$ (#1) is observed at -270 ppm; a small shoulder is observed at -800 ppm. The intensity of the main peak increases with the delay time and saturates at 2500 ms. The main peak of $^{125}$Te NMR for $Bi_2Te_3$ (#2) is observed at -180 ppm; a moderate shoulder is observed at -660 ppm. The peak position is determined not only by the chemical shift due to effects from local environment, but also by the Knight shifts due to effects from free charge carrier concentration).[25,26] In $Bi_2Te_3$ samples #1 and #2, different peak position is mostly due to the Knight shift, which agrees well with different free (mobile) carrier concentrations; this is supported by the Hall effect measurements (Table 2). The intensity of the peak also increases with the delay time and saturates at 600 ms, i.e. much faster than $Bi_2Te_3$ (#1). Small distortion of NMR spectra observed at the left of the main peak for short delay times shows a contribution from some Te in $Bi_2Te_3$ (#2).

$^{125}$Te NMR spectra of both our $Bi_2Te_3$ samples shown on Figs. 3a,b demonstrate the presence of Te atoms in different environments: the main peak from Te atoms surrounded mostly

by Bi and the right shoulder from Te close to antisite defects. The ratio of intensities of the main peak and defect sites is ~16 for sample #1 and ~6 for sample #2. The ratio between these values is ~2.6, which is close to the ratio of the carrier concentration in samples #2 and #1, ~2.5, i.e., the right shoulders reflect the carrier concentration produced by antisite defects.

Figures 4a and 4b show $^{125}$Te NMR spectra for both $Bi_2Te_3$ samples with the signal intensities rescaled to the value obtained for the saturated spectra. The spectra for $Bi_2Te_3$ (#1) do not change, in general, their shape and frequencies, i.e. there is no significant amount of Te which can produce a signal at higher and particularly at lower frequencies. In contrast, the spectra for $Bi_2Te_3$ (#2) shows some contribution to the signal at both the lower and higher frequencies, forming the left and right shoulders. The right shoulder is similar to that observed for $Bi_2Te_3$ (#1), but has larger intensity, whereas the left shoulder was not observed for $Bi_2Te_3$ (#1) (Fig. 3).

The resonance frequency, i.e. the total shift of NMR signal position, $\delta_{total}$ , relative to a reference, is the sum of the chemical shift, $\delta_{chem}$, due to chemical environment, and the Knight shift, $K$, due to a hyperfine interaction between nuclei and free charge carriers.[25,26] The different signal resonance frequencies observed for $Bi_2Te_3$ samples #1 and #2 suggest different chemical and/or Knight shifts, which, in principle, can be tested by spin-lattice relaxation measurements. Note that nuclei relaxation in metals and semiconductors is mostly determined by the hyperfine interaction of nuclei with free charge carriers [26] and affect the signal position via the Knight shift, which depends on $T_1$ via the Korringa relation $K^2T_1T = const$ , $T$ is the absolute temperature, or $K^2T_1 = const$ at a given temperature.[27] In complex tellurides the Korringa relation at a given temperature can be used for estimation of possible Knight shift vs. measured $T_1$.

When spin-lattice relaxation contains one component, fitting of the dependence of the normalized peak intensity on the saturation recovery time can be conducted by the equation [7,18]

$$I(t) = 1 - e^{-t/T_1} \quad (1)$$

However, multicomponent tellurides typically are chemically and electronically inhomogeneous and spin-lattice relaxation may contain at least two components and normalized peak intensity vs. saturation recovery time requires a bi-exponential fit

$$I(t) = f_A(1 - e^{-t/T_{1,A}}) + f_B(1 - e^{-t/T_{1,B}}) \quad (2)$$

where $f_A$ and $f_B$ are fractions of components *A* and *B* in the material, and $T_{1,A}$ and $T_{1,B}$ are the spin-lattice relaxation times of these components. [7,18]

In addition, relaxation processes can be described by the stretched exponential relaxation function.[10,20,28] This function can be used to describe $^{125}$Te NMR spin-lattice relaxation tellurides via the equation

$$I(t) = I_0\left(1 - \exp\left(\frac{t}{T_1}\right)^{\beta}\right) \quad (3)$$

where β is the Kohlrausch exponent; this equation was used to fit $^{125}$Te NMR for $Bi_2Te_3$ and related materials.[10,20] We test all three equations to describe $^{125}$Te NMR spin-lattice relaxation in our $Bi_2Te_3$ samples.

Figure 5a shows normalized intensity of $^{125}$Te NMR signal vs. saturated recovery time (delay time) for the peak for $Bi_2Te_3$ (#1); the value of $T_1$ for the main signal (peak) obtained from the plots is 300 ms. However, the peak for $Bi_2Te_3$ (#1) can be fit by two components (Eq. 2), short relaxation component with $T_{1,A}$ = 100 ms and long component with $T_{1,B}$ = 700 ms, of the same fractions, 0.5. The inset in Fig. 5a shows dependence of 1-*I*, where *I* is the intensity of $^{125}$Te NMR signal, vs. saturation recovery time (delay time) and also demonstrates the existence

of two relaxation components. The intensities of the right shoulder for $Bi_2Te_3$ (#1) as well as the left shoulder for $Bi_2Te_3$ (#2) are too small to perform a reliable quantitative analysis of its changes with delay time, but it is clear that they can be attributed to Te in the environment with $T_1$ longer and shorter, respectively, compared to that of the main peak.

Figure 5b shows normalized intensity of $^{125}$Te NMR signal vs. saturated recovery time (delay time) for the peak for $Bi_2Te_3$ (#2); the value of $T_1$ for the main signal (peak) and the shoulder obtained from the plots are 70 and 300 ms. The peak can be fit also by one component (Eq. 1) with $T_1$ = 70 ms whereas the shoulder can be fit by two components (Eq. 2), a short component with $T_{1,A}$ = 100 ms and long component with $T_{1,B}$ = 800 ms, of the same fractions, 0.5. The inset in Fig. 5b shows dependence of 1-$I$ for the peak and shoulder and confirms one component for the peak and two components for the shoulder. The peak for $Bi_2Te_3$ (#2) also can be fit by Eq. 3 with $T_1$ = 70 ms and $\beta = 1$, i.e., it can also be fit by Eq. 1. Note that Eq. 3 cannot provide good fit for the main peak for $Bi_2Te_3$ (#1) and for the right shoulder for $Bi_2Te_3$ (#2), which limits its application to our $Bi_2Te_3$ samples.

Earlier, it was shown that the carrier concentration in GeTe-based materials can be obtained using known carrier concentration and $T_1$ values in GeTe.[7,8] Both our $Bi_2Te_3$ samples (and likely all $Bi_2Te_3$ samples [3,11]) show multicomponent spin-lattice relaxation due to atomic defects, which generate free charge carriers and form electronically inhomogeneous systems. It is important to understand how the values of the carrier concentrations derived from $^{125}$Te NMR spin-lattice relaxation measurements in electronically inhomogeneous materials (differential parameters) are relevant to the value obtained from the Hall effect (integral parameter), and how these values are relevant to the Seebeck coefficient (integral parameter).

To calculate the carrier concentration in $Bi_2Te_3$ samples, a reference electronically homogeneous material with known carrier concentration and $T_1$ is needed. If GeTe is used as a reference, the carrier concentration in both $Bi_2Te_3$ samples obtained using Maxwell-Boltzmann ( $1/T_1 \sim n$) or Fermi-Dirac ($1/T_1 \sim n^{2/3}$) statistics [8,25,26] for all $T_1$ values obtained from experiment by fitting (Table 2) is, in general, much lower than that obtained from the Hall effect; this means that GeTe cannot be used as reference.

On the other hand, we can estimate the value of $T_1$, which can be attributed to the carrier concentration obtained from the Hall effect using ratios between the Seebeck coefficients, carrier concentrations, and $T_1$. The ratios between the Seebeck coefficients and free carrier concentrations in $Bi_2Te_3$ (#1) and $Bi_2Te_3$ (#2) samples can be written as $S_{\#1}/S_{\#2} = \left(n_{\#2}/n_{\#1}\right)^{2/3}$, where $S_{\#1}$ and $n_{\#1}$, $S_{\#2}$ and $n_{\#2}$ are the Seebeck coefficients and carrier concentrations of $Bi_2Te_3$ (#1) and $Bi_2Te_3$ (#2) samples, respectively. Using Maxwell-Boltzmann statistics for the analysis of the Seebeck coefficient via NMR data, this ratio can be written as $S_{\#1}/S_{\#2} = \left(T_{1,\#2}/T_{1,\#1}\right)^{2/3}$. The challenge is what $T_1$ values should be used in this estimation.

It is clear that separate $T_{1,A}$ and $T_{1,B}$ values for both samples cannot be used in calculations, and the challenge is if the average $T_1$ value calculated for each sample will be acceptable. The average values of spin-lattice relaxation time, $T_{1,av}$, can be calculated separately for the main peak and the right shoulder as $T_{1,av} = (T_{1,A})(f_A)+(T_{1,B})(f_B)$ (see Table 2). For $Bi_2Te_3$ (#1), spin-lattice relaxation time, $T_{1,\#1}$, calculated based on only the data for the main peak (the right shoulder is too small to be analyzed), will be the same as $T_{1,av}$, i. e. $T_{1,\#1}$ = 400 ms. For $Bi_2Te_3$ (#2), $T_{1,\#2}$ should be calculated using spin-lattice relaxation time values for both the main peak, 70 ms, and $T_{1,av}$ for the shoulder, 450 ms (Table 2).

Based on the intensities of the main peak and shoulder for $Bi_2Te_3$ (#2) (72 and 28%, respectively), $T_{1,\#2}$ = 176 ms. Hence, $\left(T_{1,\#1} / T_{1,\#2}\right)^{2/3}$ = (400 ms/176 ms)$^{2/3}$ = 1.73, which is just slightly smaller than $S_{\#1} / S_{\#2}$ = 1.88 (see above) and $\left(n_{\#2} / n_{\#1}\right)^{2/3}$ = 1.84. If Fermi-Dirac statistics is used for calculations, $T_{1,\#1} / T_{1,\#2}$ = 400 ms/176 ms = 2.27, which is larger compared to the value obtained using Maxwell-Boltzmann statistics. Both statistics show that the average values of spin-lattice relaxation times can, in general, be used for estimation of the free carrier concentrations in electronically inhomogeneous materials, but Maxwell-Boltzmann statistics provide a better fit with experimental values of the Seebeck coefficients and carrier concentration obtained from the Hall effect.

It also is clear that electronic inhomogeneity in complex tellurides can affect electronic and thermal transport, but the number of experimental methods, which can detect such inhomogeneity, is quite limited. For example, microscale Seebeck coefficient scanning demonstrates dramatic changes in the value and even in sign of the Seebeck coefficient of PbTe alloyed with Ag and Sb.[29] Because XRD of these materials shows a single phase, such changes were explained by slight local variations in composition. Note that PbTe and GeTe represent self-doping semiconductors, where the charge carrier concentration can be changed by the Pb/Te and Ge/Te ratio, and in addition the replacement of Ge in GeTe by Ag or Sb can decrease or increase the carrier concentration and result in electronic inhomogeneity in the case of Sb. [8]

Electronic inhomogeneity in PbTe- and GeTe-based materials at the atomic level also was detected by $^{207}$Pb and $^{125}$Te NMR. [5,8,18] $^{125}$Te NMR shows that even *p*- and *n*-types PbTe samples are electronically inhomogeneous, which reflects that the Pb/Te ratio even in PbTe is nonuniform. [18] In this study, the $^{125}$Te NMR spectra and spin-lattice relaxation measurements also demonstrate that both $Bi_2Te_3$ samples are electronically inhomogeneous at the atomic scale,

which can be attributed to a different Te environment due to spatial variation of the Bi/Te ratio resulting in various atomic defects. In general, in Bi-rich $Bi_2Te_3$ sample, $Bi_{Te}$ and/or $V_{Te}$ defects, whereas in Te-rich $Bi_2Te_3$ sample, $Te_{Bi}$ and $V_{Bi}$ defects are expected to be formed. [20,21] Hence, $^{125}$Te NMR signals observed for different $Bi_2Te_3$ single-phase samples can be produced by $Te_{(1)}$ and $Te_{(2)}$ atoms, as well as by Te close to the atomic defects, which may change their environment.

The sum of $Te_{(1)}$ and $Te_{(2)}$ atoms in $Bi_2Te_3$ (#1) and (#2) samples would be similar, and $^{125}$Te NMR main peaks in both samples can be attributed to all these Te atoms. $Bi_2Te_3$ (#1) shows *p*-type conductivity, which can be explained by the presence of mostly Bi antisite defects, $Bi_{Te}$, and in addition possibly by Bi vacancy defects, $V_{Bi}$. Note that $Bi_{Te}$ defects in $Bi_2Te_3$ synthesized from the stoichiometric melt are preferred, [3,20] and the right shoulder of small intensity in *p*-type $Bi_2Te_3$ (#1) should be attributed to Te atoms, which are close to $Bi_{Te}$ antisite defects. The hole concentration in $Bi_2Te_3$ (#1) obtained from the Hall effect is relatively low (Table 2), which agrees well with a large Seebeck coefficient (Fig. 2), and can be used as evidence for the presence of $Bi_{Te}$ antisite defects of low concentration.

$Bi_2Te_3$ (#2) shows *n*-type conductivity, which can be explained by the presence of Te antisite defects, $Te_{Bi}$; the contribution from Te vacancy defects, $V_{Te}$, is unlikely. Note that $Te_{Bi}$ defects in $Bi_2Te_3$ synthesized from the Te-rich melt are preferred, [20,21] and the right shoulder in *n*-type $Bi_2Te_3$ (#2) can be attributed to Te atoms, which are close to $Te_{Bi}$ antisite defects. The larger intensity of the shoulder in $Bi_2Te_3$ (#2) compared to that in $Bi_2Te_3$ (#1) can be explained by the higher concentration of $Te_{Bi}$. This agrees well with the higher carrier concentration obtained from the Hall effect (Table 2) and smaller absolute value of the Seebeck coefficient (Fig. 2) at 300 K.

Using our room temperature Seebeck coefficients and that reported by Satterthwaite and Ure,[30] we can suggest a likely composition of $Bi_2Te_3$ samples #1 and #2. For our *n*-type $Bi_2Te_3$ (#2), $S$ = -130 μV $K^{-1}$ can be attributed to ~63 at.% Te in melt. For *p*-type $Bi_2Te_3$ (#1), $S$ =+250 μV $K^{-1}$ is larger by ~20% compared to that for $Bi_2Te_3$ containing less than 62 at.% Te in melt. One of the reasons of such discrepancies can be different methods of the Seebeck coefficient measurements in Ref. 30 and used by us. Note also that if the amount of Te in $Bi_2Te_3$ is estimated based on the carrier concentration using our values from Table 1 and the data from Ref. 30, $Bi_2Te_3$ sample #2 may contain ~66 at.% Te, whereas #1 contains ~61 at.% Te.

$^{125}$Te NMR signal for $Bi_2Te_3$ (#2) with relatively short $T_1$ observed at the left of the main peak (Fig. 4b) should be attributed to Te located in the area with relatively high free carrier concentration. We suggest that the higher carrier concentration can be attributed to small amount of Te atoms close to $V_{Bi}$; electron configurations of Bi ($6p^3$) and Te ($5p^2$) show that each Bi vacancy can generate three holes, whereas $Bi_{Te}$ and $Te_{Bi}$ antisite defects generate one hole and one electron, respectively.

Because dominant free charge carriers in $Bi_2Te_3$ (#2) are electrons, the holes generated by $V_{Bi}$ are compensated by electrons generated by $Te_{Bi}$ antisite defects. The NMR signal at the left of the main peak in $Bi_2Te_3$ (#1) is not detected because it is unlikely that $V_{Bi}$ in this sample can be formed. It should also be noted here that the resonance frequency of all $^{125}$Te NMR signals, observed for our $Bi_2Te_3$ samples and its dependence on delay time are determined by the interplay between the chemical and Knight shifts and can be assigned to Te in environments with different local composition and free carrier concentration formed by atomic defects.

## 4. SUMMARY

Two single crystalline samples of $Bi_2Te_3$ grown (i) using Bridgman technique, sample $Bi_2Te_3$ (#1), and (ii) out of Te-rich high temperature flux, $Bi_2Te_3$ (#2), have been studied. XRD patterns show that both samples are single-phase. At 300 K, the value of the Seebeck coefficient of $Bi_2Te_3$ (#1) is positive, +250 μV $K^{-1}$ (*p*-type), whereas that of $Bi_2Te_3$ (#2) is negative, -133 μV $K^{-1}$ (*n*-type), and agrees well with the Hall effect data showing lower hole concentration and higher electron concentration, respectively. $^{125}$Te NMR for both samples show a peak and shoulder, which reflect the presence of Te in different environments. $^{125}$Te NMR spin-lattice relaxation measurements show that the peak in $Bi_2Te_3$ (#1) can be fit by two components spin-lattice relaxation time, $T_{1,A}$ and $T_{1,B}$. The intensity of the shoulder in $Bi_2Te_3$ (#1) is too small to be fit. The peak observed for $Bi_2Te_3$ (#2) can fit by one $T_1$ component, whereas the shoulder can be fit by two components; this means both materials are electronically inhomogeneous. $^{125}$Te NMR peaks observed for both $Bi_2Te_3$ (#1) and $Bi_2Te_3$ (#2) can be attributed to the majority of Te atoms surrounded by Bi, whereas the shoulders to Te atoms close to $Bi_{Te}$ or $Te_{Bi}$ antisite defects, respectively. $^{125}$Te NMR spectroscopy and spin-lattice relaxation measurements is an effective probe to study antisite defects in $Bi_2Te_3$ and related tellurides, and along with the Seebeck coefficient measurements enable better understanding of their effect on electronic transport.

AUTHOR INFORMATION
Corresponding Author
E-mail levin@iastate.edu, Tel: 1-515-294-6093 (E.M.L.)

Notes
The authors declare no competing financial interest

ACKNOWLEDGEMENTS

Authors thank the Materials Preparation Center at the Ames Laboratory U.S. Department of Energy (DOE) for sample synthesis. This work was supported by the U.S. Department of Energy, Office of Basic Energy Sciences, Division of Materials Sciences and Engineering. The research was performed at the Ames Laboratory, which is operated for the U.S. Department of Energy by Iowa State University under Contract No DE-AC02-07CH11358.

REFERENCES

(1) Goldsmid, H. J. *Thermoelectric refrigeration*. Springer, Science + Business Media, New York, **1964**.

(2) Hasan M. Z.; Kane, C. L. Topological insulators. *Rev. Mod. Phys*. **2010**, *82*, 3045-3067.

(3) Scanlon, D. O.; King, P. D. C.; Singh, R. P.; De la Torre, A.; McKeown Walker, S.; Balakrishnan, G.; Baumberger, F.; Catlow, C. R. A. Controlling bulk conductivity in topological insulators: key role of anti-site defects. *Adv. Mater*. **2012**, *24*, 2154-2158.

(4) Alexander, M. N.; Sagalyn, P. L.; Senturia, S. D.; Hewes, C. R. Nuclear spin relaxation study of the electronic structure of lead telluride. *J. Nonmetals* **1973**, *1*, 251-256.

(5) Levin, E. M.; Cook, B. A.; Ahn, K.; Kanatzidis, M. G.; Schmidt-Rohr, K. Electronic inhomogeneity and Ag:Sb imbalance of $Ag_{1-y}Pb_{18}Sb_{1+z}Te_{20}$ high-performance thermoelectrics elucidated by $^{125}$Te and $^{207}$Pb NMR. *Phys. Rev. B* **2009**, *80*, 115211.

(6) Levin, E. M.; Besser, M. F.; Hanus, R. Electronic and thermal transport in GeTe: a versatile base for thermoelectric materials. *J. Appl. Phys*. **2013**, *114*, 083713.

(7) Levin, E. M.; Hanus, R.; Hanson, M.; Strazsheim, W.; Schmidt-Rohr, K. Thermoelectric properties of $Ag_2Sb_2Ge_{46-x}Dy_xTe_{50}$ alloys with high power factor. *Physica Status Solidi A* **2013**, *210*, 2628-2637.

(8) Levin, E. M. Effect of Ge substitution in GeTe by Ag or Sb on the Seebeck coefficient and carrier concentration derived from $^{125}$Te NMR. *Phys Rev B* **2016**, *93*, 045209.

(9) Taylor, R. E.; Leung, B.; Lake, M. P.; Bouchard, L.-S. Spin-lattice relaxation in bismuth chalcogenides. *J. Phys. Chem. C* **2012**, *116*, 17300-17305.

(10) Koumoulis, D.; Chasapis, T. C.; Taylor, R. E.; Lake, M. P.; King, D.; Jarenwattananon, N. N.; Fiete, G. A.; Kanatzidis, M. G.; Bouchard, L.-S. NMR probe of metallic states in nanoscale topological insulators. *Phys. Rev. Lett*. **2013**, *110*, 026602.

(11) Fleurial, J. P.; Gailliard, L.; Triboulet, R.; Scherrer H.; Scherrer, S. Thermal properties of high quality single crystals of bismuth telluride-part I: experimental characterization. *J. Phys. Chem. Solid* **1988**, *49*, 1237-1247.

(12) Canfield, P. C.; Kong, T.; Kaluarachi, U. S.; Jo, N. H. Use of frit-disc crucible for routine and exploratory solution growth of single crystalline samples. *Philos. Mag. B* **2016**, *96*, 84-92.

(13) Canfield, P. C.; Fisk, Z. Growth of single crystals from metallic fluxes. *Philos. Mag. B* **1992**, *65*, 1117-1123.

(14) ASM Alloy Phase Diagram Database: www1.asminternational.org/ (accessed June 10, 2016).

(15) Wang, G.; Endicott, L.; Uher, C. In *Thermoelectric $Bi_2Te_3$ Nanomaterials*. Willey-VCH, Ed. by Eible, O.; Nielsch, K.; Peranio, N.; Volklein, F. Weinheim, Germany, **2015**. Ch. 5, p. 73-98.

(16) Nakajima, S. J. The crystal structure of $Bi_2Te_{3-x}Se_x$. *J. Phys. Chem. Solids* **1963**, 24, 479-485.

(17) Yavorsky, B. Yu.; Hinsche, N. F.; Mertig, I.; Zahn, P. Electronic structure and transport anisotropy of $Bi_2Te_3$ and $Sb_2Te_3$. *Phys. Rev. B* **2011**, *84*, 165208.

(18) Levin, E. M.; Heremans, J. P.; Kanatzidis, M. G.; Schmidt-Rohr, K. Electronic inhomogeneity in *n*- and *p*-type PbTe detected by $^{125}$Te NMR. *Phys. Rev. B* **2013,** *88*, 115211.

(19) Miller, G. R.; Li, C. Y. Evidence for the existence of antistructural defects in bismuth tellurides by density measurements. *J. Phys. Chem. Solids* **1965**, *26*, 173-177.

(20) Koumoulis, D.; Leung, B.; Chasapis, T. C.; Taylor, R.; King, D. Jr; Kanatzidis, M. G.; Bouchard, L.-S. Understanding bulk defects in topological insulators from nuclear-spin interactions. *Adv. Funct. Mater*. **2014**, *24*, 1519-1528.

(21) A. Hashibon, A.; Elsasser, C. In *Thermoelectric $Bi_2Te_3$ Nanomaterials*. Willey-VCH, Ed. by O. Eible, K. Nielsch, N. Peranio, and F. Volklein. Weinheim, Germany, 2015. Ch. 9, p. 167-186.

(22) Oh, M. W.; Son, J. H.; Kim, B. S.; Park, S. D.; Min, B. K.; Lee, H. W. Antisite defects in n-type $Bi_2(Te,Se)_3$: experimental and theoretical studies. *J. Appl. Phys*. **2014**, *115*, 133706.

(23) Hashibon, A.; Elsasser, C. First-principle density functional theory study of native point defects in $Bi_2Te_3$. *Phys. Rev. B* **2011**, *84*, 144117.

(24) Snyder, G. J.; Toberer, E. S. Complex thermoelectric materials. *Nature Mater*. **2008**, 7, 105-114.

(25) Selbach, H.; Kanert, O.; Wolf, D. NMR investigation of the diffusion and conduction properties of the semiconductor tellurium. I. Electronic properties. *Phys. Rev. B* **1979**, *19*, 4435-4443.

(26) Yesinowski, J. P. Solid-state NMR of inorganic semiconductors. *Top. Curr. Chem*. **2012**, *306*, 229-312.

(27) Yesinowski, J. P.; Purdy, A. P.; Wu, H.; Spencer, M. G.; Hunting, J.; DiSalvo, F. J. Distribution of conduction electrons as manifested in MAS NMR of gallium Nitride. *J. Am. Chem. Soc*. **2006**, *128*, 4952-4953.

(28) Johnston, D. C. Stretched exponential relaxation arising from a continuous sum of exponential decays. *Phys. Rev. B* **2006**, *74*, 184430.

(29) Chen, N.; Gascoin, F. G.; Snyder, G. J.; Muller, E.; Karpinski, G.; Stiewe, C. Macroscopic thermoelectric inhomogeneities in $(AgSbTe_2)_x(PbTe)_{1-x}$. *Appl. Phys. Lett*. **2005**, *87*, 171903.

(30) Satterthwaiste, C. B; Ure, Jr., R. W. Electrical and thermal properties of $Bi_2Te_3$. *Phys. Rev.* **1957**, *108*, 1164-1170.

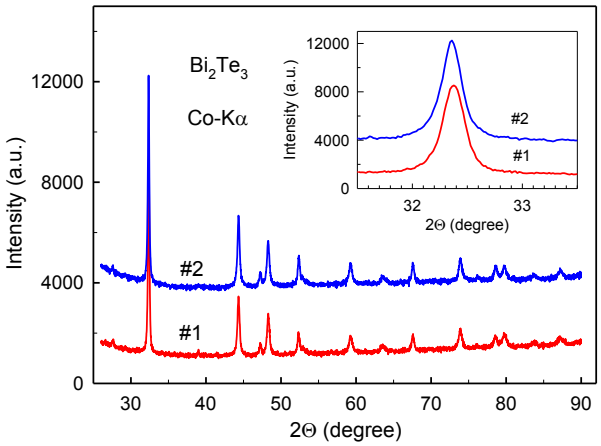


Figure 1. XRD (Co-$K_\alpha$, $\lambda = 0.1789$ nm) patterns of $Bi_2Te_3$ samples #1 and #2 at 300 K. The inset shows an expanded view for the main peak at $31.5° \leq 2\Theta \leq 33.5°$.

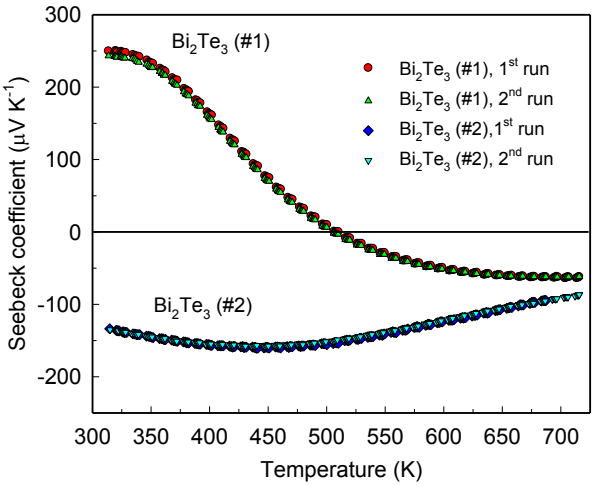


Figure 2. Temperature dependencies of the absolute Seebeck coefficient of $Bi_2Te_3$ samples #1 and #2, showing stability of the Seebeck coefficient and different type of conductivity at 300 K.

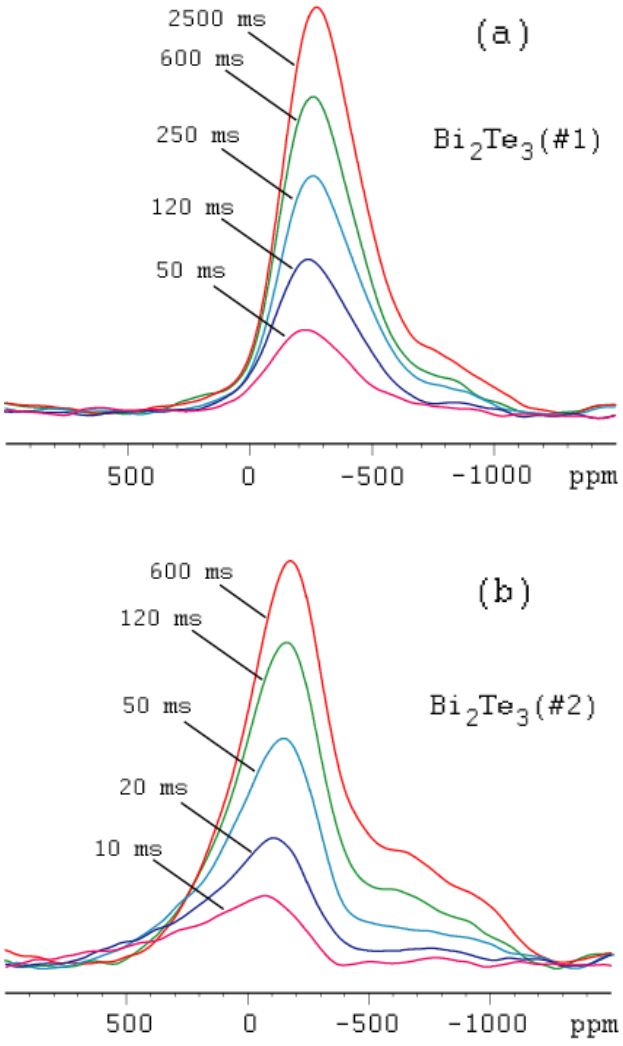


Figure 3. $^{125}$Te NMR spectra of $Bi_2Te_3$ samples (a) #1 and (b) #2 obtained at 300 K for various saturation recovery (delay) times.

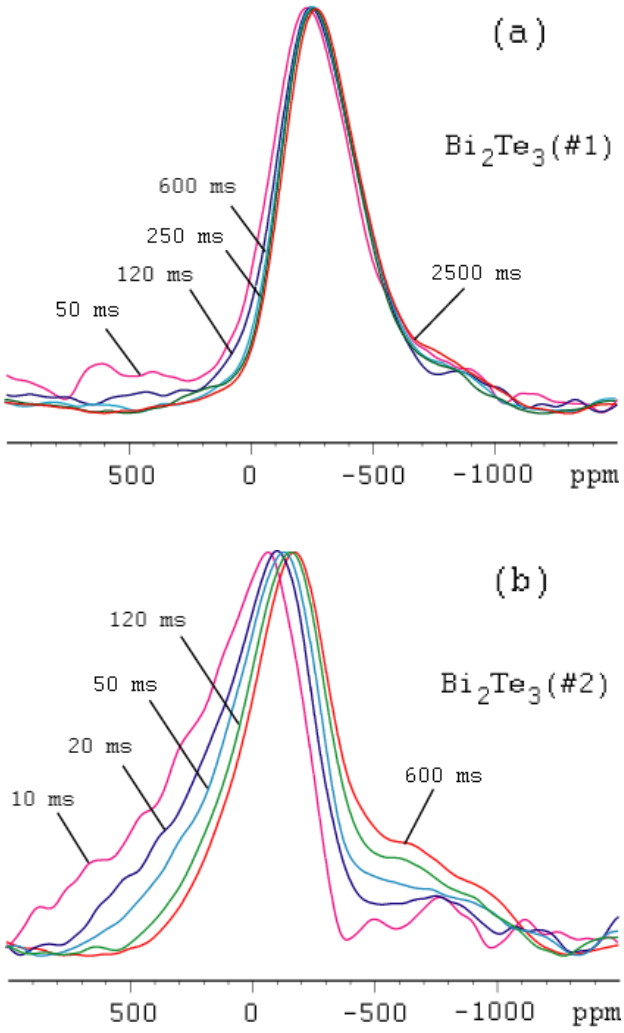


Figure 4. $^{125}$Te NMR spectra of $Bi_2Te_3$ samples (a) #1 and (b) #2 obtained at 300 K for various saturation recovery (delay) times and rescaled to the value obtained for the saturated spectra.

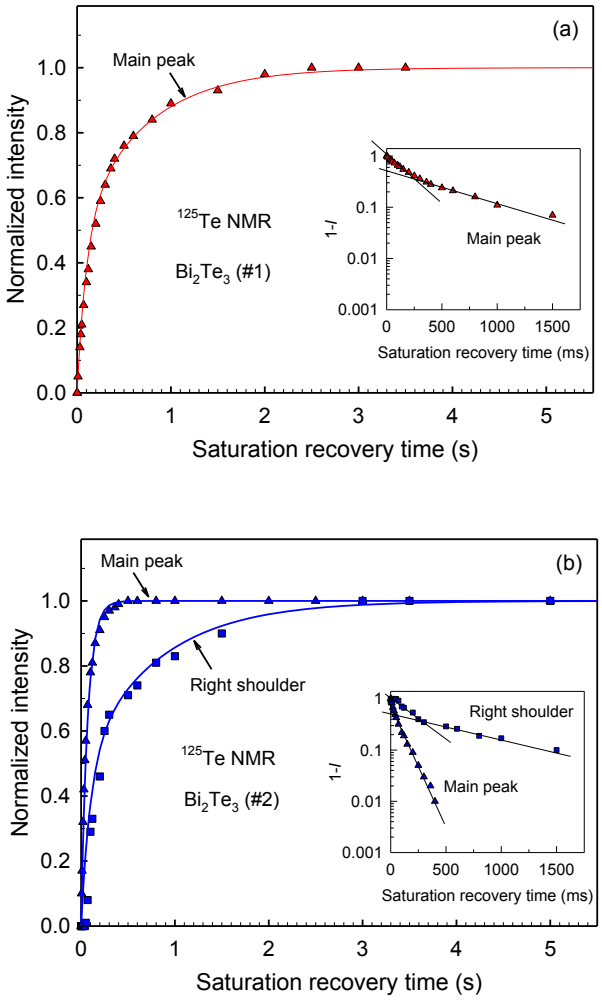


Figure 5. $^{125}$Te NMR spin-lattice relaxation for $Bi_2Te_3$ samples (a) #1 and (b) #2 at 300 K. The insets in (a) and (b) show semilogarithmic plots of (1-*I*) vs saturation recovery time, which can be fit by two spin-lattice relaxation times, $T_{1,A}$ and $T_{1,B}$, for the main peak in (a) and for the right shoulder in (b), and by one $T_1$ component for the main peak in (b). The right shoulder for $Bi_2Te_3$ (#1) (Fig. 3a) and the left shoulder for $Bi_2Te_3$ (#2) (Fig. 4b) are too small for analysis.

Table 1

Lattice parameters of $Bi_2Te_3$ samples at 300 K calculated for hexagonal and rhombohedral structures.

| Sample | Hexagonal structure | | Rhombohedral structure | |
|---|---|---|---|---|
| | $a$ (Å) | $c$ (Å) | $a = b =$ c (Å ) | $\alpha = \beta = \gamma$ (°) |
| $Bi_2Te_3$ (#1) | 4.386 | 30.509 | 10.480 | 24.16 |
| $Bi_2Te_3$ (#2) | 4.385 | 30.478 | 10.470 | 24.18 |
| $Bi_2Te_3$ | 4.386[a] | 30.497[a] | 10.473[b] | 24.17[b] |

a - Ref. 16
b - Ref. 17

Table 2

$^{125}$Te NMR main peak and right shoulder positions, spin-lattice relaxation time, $T_1$, Seebeck coefficient, and carrier concentration obtained from the Hall effect for $Bi_2Te_3$ samples at 300 K.

| Sample | $^{125}$Te NMR signal position (ppm) | | Spin-lattice relaxation time, $T_1$ | | Seebeck coefficient ($\mu$V K$^{-1}$) | Carrier concentration from Hall effect ($\times 10^{19}$ cm$^{-3}$) |
|---|---|---|---|---|---|---|
| | Peak | Right shoulder | Peak | Right shoulder | | |
| $Bi_2Te_3$ (#1) | -270 | -800 | $T_{1,A}$=100 ms, $f_A$=0.5<br>$T_{1,B}$=700 ms, $f_B$=0.5<br>$T_{1,av}$=400 ms | Too small intensity | +250 | 1.2 (*p*-type) |
| $Bi_2Te_3$ (#2) | -180 | -660 | $T_1$=70 ms | $T_{1,A}$=100 ms, $f_A$=0.5<br>$T_{1,B}$=800 ms, $f_B$=0.5<br>$T_{1,av}$=450 ms | -133 | 3.0 (*n*-type) |